A Time-Resolved Iron-Specific X-ray Absorption Experiment Yields No Evidence for an $Fe^{2+} \rightarrow Fe^{3+}$ Transition during $Q_A^- \rightarrow Q_B$ Electron Transfer in the Photosynthetic Reaction Center†

Sabine Hermes,‡ Oliver Bremm,‡ Florian Garczarek,‡ Valerie Derrien,§ Peter Liebisch,|| Paola Loja,|| Pierre Sebban,§ Klaus Gerwert,*,‡ and Michael Haumann*,||

Lehrstuhl für Biophysik, ND 04/596, Ruhr-Universität Bochum, D-44801 Bochum, Germany, FB Physik, Arnimallee 14, Freie Universität Berlin, D-14195 Berlin, Germany, and Laboratoire de Chimie-Physique, UMR 8000, Bât. 350, Faculté d'Orsay, 91405 Orsay Cedex, France

Received August 9, 2005; Revised Manuscript Received November 10, 2005

ABSTRACT: Previous time-resolved FTIR measurements suggested the involvement of an intermediary component in the electron transfer step $Q_A^- \rightarrow Q_B$ in the photosynthetic reaction center (RC) from *Rhodobacter sphaeroides* [Remy and Gerwert (2003) *Nat. Struct. Biol. 10*, 637]. By a kinetic X-ray absorption experiment at the Fe K-edge we investigated whether oxidation occurs at the ferric non-heme iron located between the two quinones. In isolated reaction centers with a high content of functional Q_B, at a time resolution of 30 μs and at room temperature, no evidence for transient oxidation of Fe was obtained. However, small X-ray transients occurred, in a similar micro- to millisecond time range as in the IR experiments, which may point to changes in the Fe ligand environment due to the charges on Q_A^- and Q_B^-. In addition, VIS measurements agree with the IR data and do not exclude an intermediate in the $Q_A^- \rightarrow Q_B$ transition.

The photosynthetic bacterial reaction center (BRC)[1] represents one of the best studied bioenergetic model systems both with respect to its structural characterization by crystallography (*1*) and with respect to the elucidation of its light-driven electron and proton transfer reactions (*2*). In the RC from the purple non-sulfur bacterium *Rhodobacter sphaeroides*), the absorption of light induces a charge separation within about 200 ps leading to the formation of the P^+/Q_A^- pair where P^+ denotes an oxidized bacteriochlorophyll molecule and Q_A^- the reduced primary ubiquinone-10 (UQ_{10}) tightly bound to the M-subunit (*3*). Electron transfer to the secondary quinone Q_B in the L-subunit then occurs on the micro- to millisecond time scale (*3*). A second photon induces the double reduction and protonation of Q_B^-, whereafter the quinol is released from the RC.

Nevertheless, a central question is insufficiently understood, namely, how the light-induced electron transfer involving the quinones couples to proton uptake. This process is crucial in the energy transduction. Several amino acid residues which change their protonation state have been identified by site-directed mutagenesis (*2*−*4*). The first reduction of Q_B has been postulated to be conformationally gated by a propeller twist movement of Q_B from the so-called distal to the proximal site more deeply in the binding pocket previously observed by crystallography at cryogenic temperatures (*5*).

However, time-resolved FTIR experiments show occupation of both Q_B positions in a ratio of about 30%−70% but exclude a light-induced propeller twist movement (*6*, *7*). Accordingly, in recent investigations on BRC preparations (*8*−*10*) only the proximal site has been found to be largely occupied at room temperature. Alternatively, the rate-limiting step seems to be the protonation of residues in the proton uptake pathway leading to Q_B. This was a surprising result of recent step-scan FTIR measurements (*7*) in the time range from 30 ns to 35 s, which showed that protonation of His126 and His128 and transient protonation of Asp210 take place with time constants of 12 and 150 μs (Figure 1). Furthermore, it was elucidated, in contrast to the current paradigm, that the main portion of the reduction of Q_B seems to occur prior to the oxidation of Q_A^- (*7*). At 278 K the appearance of IR marker bands for Q_B^- predominantly occurred with a time constant τ_1 of about 150 μs, whereas the disappearance of the rapidly formed IR bands attributable to Q_A^- mainly was significantly slower, $\tau_2 = 1.1$ ms. These IR marker bands previously had been identified by isotopic labeling (*6*, *11*, *12*). This observation has been interpreted in terms of a preceding reduction of Q_B by the oxidation of an unknown intermediary electron donor, which only thereafter was rereduced by Q_A^- (*7*). Whereas the evidence for reduction

† Financial support from the Deutsche Forschungsgemeinschaft by Grant SFB498-C8 to M.H. and SFB480-C3 to S.H. and K.G. is gratefully acknowledged.

* To whom correspondence should be addressed. M.H.: tel, +49 30 8385 6101; fax, +49 30 8385 6299; e-mail, haumann@physik.fu-berlin.de. K.G.: tel, +49 234 3224461; fax, +49 234 3214238; e-mail, gerwert@bph.rub.de.

‡ Ruhr-Universität Bochum.

§ Laboratoire de Chimie-Physique.

|| Freie Universität Berlin.

[1] Abbreviations: BRC, bacterial reaction center; EPR, electron paramagnetic resonance spectroscopy; Fe, iron; Mn, manganese; FTIR, Fourier transform infrared spectroscopy; LDAO, lauryldimethylamine oxide; P^+, oxidized primary donor; $Q_{A,B}$, quinones bound to the BRC; Tris, tris(hydroxymethyl)aminomethane; VIS, electronic absorption in the visible spectral region; XANES, X-ray absorption near edge structure; XAS, X-ray absorption spectroscopy.

10.1021/bi0515725 CCC: $33.50
Published on Web 12/15/2005

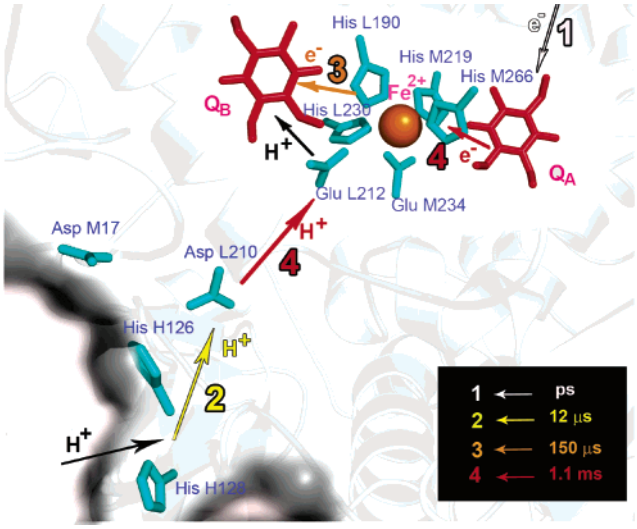

FIGURE 1: View of the environment where the Q_A^- to Q_B electron transition takes place (PDB entry 1AIG; Pymol). The Fe(II) is depicted in orange. Amino acid residues possibly involved in proton transfer from the protein surface and amino acid ligands to the Fe ion are shown in cyan. Quinones at the Q_A and Q_B binding sites are shown in red. Secondary structure elements of the L, M, and H subunit sliced for a view into the Q_A and Q_B binding sites are illustrated in gray. Colored arrows describe the events of proton and electron transport with their respective time constants, as observed by FTIR (*7*). Black arrows indicate proton uptake at the protein surface and final proton transfer to Q_B after its double reduction by a second electron.

of Q_B prior to Q_A^- oxidation seemingly was clear-cut, the chemical nature of the intermediate remained unclear. One tempting option, based on the structural model shown in Figure 1, is that the ferric non-heme iron [Fe(II)] functions as a transient electron donor/acceptor. It is coordinated by four histidines and one glutamate residue and positioned just between the two quinones (*1*).

How electron transfer in the BRC is affected by the Fe(II) is not fully clear. Earlier experiments with Fe-depleted BRC (apo-RC) revealed the decay of the yield of Q_A^-, significant slowing of the $Q_A^- \rightarrow Q_B$ step, now exhibiting pronounced nonexponential reaction kinetics (*13*), and a slowing of the primary charge separation by a factor of ~15 (*14*). There was residual $Q_A^- \rightarrow Q_B$ electron transfer in apo-RC (*13*, *15*); however, there were also uncertainties with respect to the residual Fe content of preparations and to the integrity of the RC after the depletion treatments (*16*). The transient oxidation of the Fe(II) may be hard to detect in kinetic UV−VIS experiments due to its weak absorption (*17*), real-time ^{57}Fe-specific Mössbauer spectroscopy currently is not possible (*18*), and transient EPR spectroscopy is hampered by the superimposition of signals from P^+ and Q_A^- and by the magnetic coupling of Q_A^- to the paramagnetic high-spin Fe(II) (*19*).

In this study, we investigated the possible redox reaction of the non-heme iron of the RC from *Rb. sphaeroides* by a kinetically competent and fully Fe-specific technique, namely, time-resolved X-ray absorption spectroscopy (XAS) (*20*) at the Fe K-edge. The position of the K-edge on the X-ray excitation energy scale is highly sensitive to the oxidation state of the Fe. Using previously established procedures for XAS at room temperature (*20*, *31*), the oxidation state of the Fe on the time scale of the $Q_A^- \rightarrow Q_B$ electron transfer was monitored with a resolution of 30 μs. The experimental results and their implications for the $Q_A^- \rightarrow Q_B$ transition will be discussed. In addition, we examined the $Q_A^- \rightarrow Q_B$ electron transfer by VIS measurements in RC preparations where the native Fe atom was present and in preparations where the iron was replaced by manganese to complement the previous FTIR results.

MATERIALS AND METHODS

Sample Preparation. Wild-type RC protein containing an iron atom at the acceptor side was purified from *Rb. sphaeroides* as described (*7*) and concentrated to ~500 μM using a microconcentrator (Pall Filtron, MWCO 30 kDa) as calculated from the measured absorbance at 802 nm and $\epsilon_{802} = 0.288\ \mu M^{-1}\ cm^{-1}$ (*21*). Quinone reconstitution was achieved by incubating the BRC with 10 mg/mL UQ_{10} (Sigma) for 24−48 h. By atomic absorption spectroscopy performed in the laboratory of Dr. K. Irrgang (TU-Berlin), a content of 1.0 ± 0.1 Fe BRC protein was determined. Protein solution containing 300 μg of RC was pipetted onto a Kapton window and partially dried in the dark under a gentle nitrogen stream. Samples were stored in liquid nitrogen until use. Three types of BRC samples were investigated: (1) unsealed BRC open to the X-ray beam, (2) sealed BRC covered by a Kapton foil, and (3) liquid BRC solution (no drying of protein was involved) in a Kapton cuvette.

For RC preparations where the iron was replaced by manganese, *Rb. sphaeroides* cells were grown in malate yeast medium supplemented with kanamycin (20 μg/mL) and tetracyclin (2 μg/mL). $FeSO_4 \cdot H_2O$ (7 mg) was replaced by 30.8 mg of $MnSO_4 \cdot H_2O$ in the growth medium. The cultures were grown in darkness at 30 °C. Purification of the RC protein was done as described previously (*37*). By total-reflection X-ray fluorescence analysis (TXRF) (*38*) performed at Röntec (Berlin) a content of 0.98 ± 0.07 Mn ions per RC was determined.

Kinetic Optical Absorption Measurements. P^+/Q_A^- and P^+/Q_B^- charge recombination was monitored at 960 nm using a home-built flash spectrophotometer at 291 K (*22*) at the synchrotron in the same samples as employed for XAS. Absorption kinetics were fitted by the sum of two exponentials. Q_A^- and Q_B^- formation/decay was followed at 278 K and at 291 K at two wavelengths, 460 and 440 nm, with 2−5 μM RC in 10 mM Tris, 1 mM EDTA, and 0.025% LDAO, pH 8.0. Light flashes (20 ns, 530 nm, ~5 mJ) were provided by an eximer-pumped fluorescent dye, coumarin-153 (Eximer Laser LPX 340i; Lambda Physik). Measuring wavelengths were selected by appropriate interference filters. The output of the detector photomultiplier was recorded by a LeCroy digital storage oscilloscope (model 9304M) and on a PC equipped with an Adwin8F A/D card on different time scales.

X-ray Absorption Experiments. X-ray spectroscopy at the Fe K-edge was performed at the European Synchrotron Radiation Facility (ESRF, Grenoble, France) at undulator beamline ID26 (*23*). The excitation energy (accuracy ±0.5 eV) was chosen by scanning of the monochromator (Si220 crystal); the gaps of two undulators were set at fixed energies spaced by about 30 eV, yielding a flat X-ray intensity profile in the Fe K-edge region. The incident X-ray intensity, I_0, was monitored in front of the sample by a detector foil. The

excited X-ray fluorescence, I_F, was monitored perpendicular to the incident beam by a scintillation detector (19.6 cm^2 active area, 51 BMI/2E1-YAP-Neg from Scionix; ~50% conversion efficiency, shielded by 10 μm Mn and 2 μm Al filters against scattered X-rays and visible light). The current output of the fast detector photomultiplier was converted to a voltage via a 20 kΩ working resistor. Thereafter, the detector output signal was branched. (i) For the time-resolved detection of X-ray fluorescence changes at fixed excitation energy (time scan of X-ray fluorescence), the signal was amplified 30-fold by a DC to 10 MHz preamplifier, limited to 30 kHz electrical bandwidth by a Tektronix amplifier, and recorded at 300 kHz sampling rate on a PC equipped with a 20 MHz A/D card (Adlink) and homemade data acquisition software. (ii) For rapid-scan XANES measurements (*24*), the signal was amplified by the beamline electronics, and spectra were recorded by continuous scanning of the X-ray energy from 7105 to 7155 eV within 0.5−1 s using the software available at the beamline. XANES spectra represent X-ray intensities I_F/I_0 normalized to 100% edge jump with respect to a spectrum measured over a longer energy range of 7000−7800 eV (not documented) and normalized as previously described (*25*). An energy calibration (accuracy ±0.2 eV) was performed on the basis of the second derivative of the spectrum of an Fe foil placed about 1 m behind the sample which was measured simultaneously in absorption mode. By XANES scans on empty sample holders we assured the absence of Fe contaminations in the X-ray beam.

Calibration of X-ray fluorescence time scan transients from BRC samples with respect to the Fe K-edge amplitude was performed as follows. Before and after the measurements employing flash excitation, a time scan was performed at 7110 eV and at 7130 eV. The two measurements at each excitation energy were averaged to account for the small decrease of the X-ray intensity due to beam loss in the storage ring during the flash measurements (<2%) to obtain about the zero level at 7110 eV and a value close to the maximum of the Fe K-edge at 7130 eV. The respective fluorescence levels were compared to the normalized XANES spectrum, thereby providing amplitude calibration of the flash transients.

BRC samples exposed to plain air of 291 K in darkness were positioned in the X-ray beam (spot size ~1 × 2 mm^2, X-ray flux ~5 × 10^{12} s^{-1} mm^{-2}) at an angle of 45° between the electric field vector of the linearly polarized X-ray beam and the sample normal by a computer-controlled sample changer. During the time scans of X-ray fluorescence, samples were illuminated by a single flash from a Q-switched, frequency-doubled Nd:YAG laser (Continuum Minilite-II, λ = 532 nm, ~20 mJ per 5 ns pulse, spot size ~7 mm^2). The spacing interval between flashes was 20, 30, or 45 s to allow for complete recombination of the P^+/Q_A, P^+/Q_B^- pairs (*7*). Between the laser flashes, the X-ray beam was blocked by a rapid photoshutter, which opened only for a time interval of 5 ms prior to and until 45 ms after the flash. Data acquisition was triggered on each laser flash by a photodiode.

The whole series of X-ray measurements that was recorded on a single BRC sample was as follows: (1) one XANES spectrum, (2) two time scans at 7110 and 7130 eV, (3) 10 time scans at an energy between 7122 and 7126 eV during which a laser flash was fired, (4) 100 time scans under the same conditions, (5) two time scans at 7110 and 7130 eV, and (6) one XANES spectrum. The maximal total X-ray exposure time was 7.7 s.

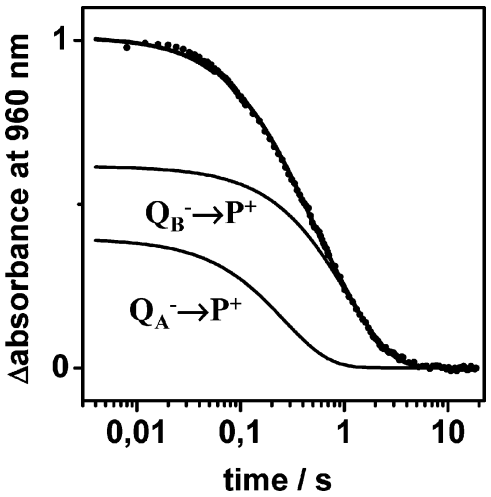

FIGURE 2: Typical flash-induced absorption transient at 960 nm of Fe-containing BRC protein attributable to rapid P^+ formation followed by its biphasic decay due to recombination with Q_A^- or Q_B^-. 120 data points were sampled on a logarithmic scale; 5 measurements at room temperature on the same sample were averaged. The flash spacing interval was 20 s to allow for complete charge recombination. Solid lines indicate a biexponential simulation and its individual kinetic phases (see text).

RESULTS

To make sure that only samples containing functional UQ_{10} at the Q_B site were investigated by XAS, its content was quantified at the beamline by flash spectrometry at 960 nm on the same BRC samples employed for the XAS experiments (Figure 2). The unresolved formation within picoseconds of P^+ was followed by a biphasic decay. Its fast and slow phases reflect P^+/Q_A^- and P^+/Q_B^- recombination (*26*). In sealed and in liquid BRC samples, dehydration was largely absent and a mean Q_B content of 60% was determined after X-ray exposure. Only those samples were subjected to further analysis. We considered the Q_B content to be sufficiently high, allowing for meaningful Fe XAS measurements. Because Q_B activity was not decreased after the XAS experiment, damage of the RC protein due to the X-ray exposure likely was absent, in accord with the XANES spectra (see below). In unsealed BRC samples the apparent Q_B content after XAS depended on the degree of dehydration of the BRC and was low. Presumably, slow dehydration of samples during the XAS measurements caused inhibition of the $Q_A^- \rightarrow Q_B$ electron transfer (*27*). These samples were not included in our analysis.

XAS experiments were performed at the Fe K-edge (Figure 3) on all three different types of BRC samples. The XANES spectrum of the non-heme iron (Figure 3A) was independent of the sample type and similar to previous ones (*28*, *29*). The magnitude of its preedge feature around 7113 eV and the large primary maximum at ~7128 eV are in line with a distorted octahedral coordination of the Fe(II) by four nitrogens from histidines and two oxygens from the carboxylic side chain of the bidentate glutamate ligand as found in the crystal structure (*1*) and with the predominant presence of two quinones (*28*). Almost identical spectra (Figure 3A) were obtained before and after the flash X-ray experiments

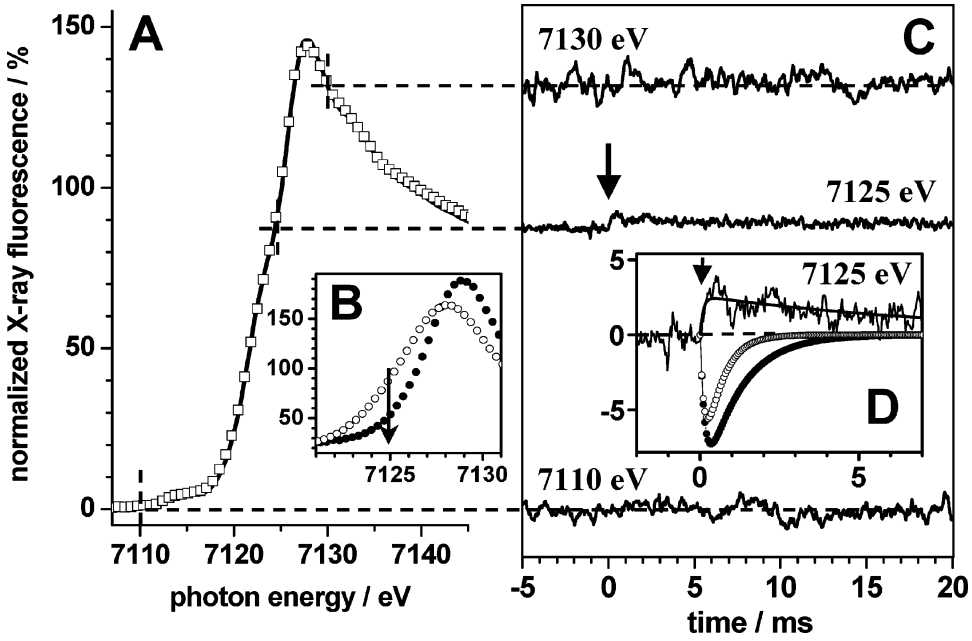

FIGURE 3: X-ray experiments at the Fe K-edge. (A) Normalized XANES spectra of the BRC protein measured by a single monochromator scan of 0.5 s before (line) and after (squares) the flash experiments. (B) XANES spectra of 5 mM aqueous solutions of $K_4[Fe^{II}(CN)_6]$ (open circles) and $K_3[Fe^{III}(CN)_6]$ (solid circles). The arrow indicates the change in the fluorescence level at 7125 eV due to the shift of the Fe(III) edge with respect to that of Fe(II). (C) X-ray fluorescence trace at 7125 eV (average of two experiments) during which one laser flash (arrow) was applied to liquid BRC samples (30 μs per point; 100 measurements were averaged). Traces at 7110 and 7130 eV (average of two measurements each; traces were smoothed over 25 data points for display) yielded amplitude calibration of the flash transient at 7125 eV when related to the respective levels of X-ray fluorescence in the XANES spectra in (A) as shown by the dashed lines. (D) The trace at 7125 eV from (C) in magnification. Symbols denote transients calculated for the hypothetical oxidoreduction of Fe using the superimposition of two rising exponentials. Key: solid circles, $A_1 = -10\%$, $\tau_1 = 150$ μs and $A_2 = +10\%$, $\tau_2 = 1.1$ ms; open circles, $A_1 = -10\%$, $\tau_1 = 130$ μs and $A_2 = +10\%$, $\tau_2 = 540$ μs. XAS measurements were performed at 291 K. The line represents a fit of the experimental trace with $A_1 = +3\%$, $\tau_1 = 100$ μs and $A_2 = -3\%$, $\tau_2 = 8.5$ ms.

described below, indicating the absence of radiation damage to the Fe site.

A Fe(II) → Fe(III) transition in a non-heme Fe compound with predominant nitrogen coordination of the metal is expected to cause a shift of the K-edge to higher energies by about 2−3 eV (*30*). An upshift by ~2 eV around edge half-height is exemplified by the XANES spectra of Fe(II) and Fe(III) in the respective hexacyano complexes (Figure 3B). In the 7122−7126 eV region, such a shift causes a decrease in the X-ray fluorescence level by up to 40% (arrow in Figure 3B). A similar decrease may be expected for a shift of the XANES spectrum of Fe(II) in the BRC due to its oxidation to Fe(III).

Figure 3C shows X-ray transients measured at excitation energies of 7130 and 7110 eV for amplitude calibration and at 7125 eV on a liquid BRC sample during which one laser flash was applied. Clearly, at 7125 eV no decrease in the fluorescence level around the flash is observed. Rather, a small positively directed change is visible. Its amplitude was variable, presumably depending on the degree of dehydration of the BRC protein in the different samples, however, not exceeding the one shown in Figure 3C. A negatively directed change of sizable magnitude was never detected in over 15 flash experiments performed on all three types of BRC samples in the energy range from 7122 to 7126 eV (not shown). This result holds both for the first 10 laser flashes where dehydration of samples presumably was small even in unsealed BRC samples and in the measurements employing the averaging of 100 flashes on sealed and liquid samples (Figure 3C). (We note that the time resolution and the sensitivity of the X-ray experiment were evaluated in measurements of the oxidation of the manganese complex of photosystem II performed during the same measuring period at the synchrotron (see ref *31* and Supporting Information). Changes in the X-ray fluorescence level of less than 10% of the normalized K-edge jump routinely were detected. In the BRC measurements at the Fe K-edge even smaller changes of less than 5% were resolved (Figure 3D).

We calculated the X-ray changes (Figure 3D) which were expected for the oxidation and subsequent reduction of the Fe(II) with time constants of 150 μs and 1.1 ms derived from FTIR at 278 K (*7*) assuming only 25% functional Q_B. Obviously, there was no indication for similar redox reactions of Fe in the experimental trace which were expected to be visible even with low Q_B contents at the used time resolution of 30 μs. A simulation (Figure 3D) with the time constants of 130 and 540 μs observable in VIS measurements (see below) at the same temperature of 291 K as used for XAS suggested that also such changes were absent in the experimental trace. A fit of the experimental trace yielded a time constant of about 100 μs for the rapid rise and of 8.5 ms for the subsequent decay of the X-ray fluorescence signal (Figure 3D, line). The small amplitude of the positively directed change in the X-ray fluorescence is compatible with a shift of the Fe K-edge by 0.1−0.2 eV to lower energies. Such an intermediate may agree with the proposed intermediate based on the IR signals (*7*). For elucidation of the origin of the X-ray transient further investigations are required.

An obvious question regarding the previous FTIR results (*7*) has appeared: If there is a transient redox intermediate, why had it not been seen in the visible spectral region in former experiments? Therefore, we investigated again the

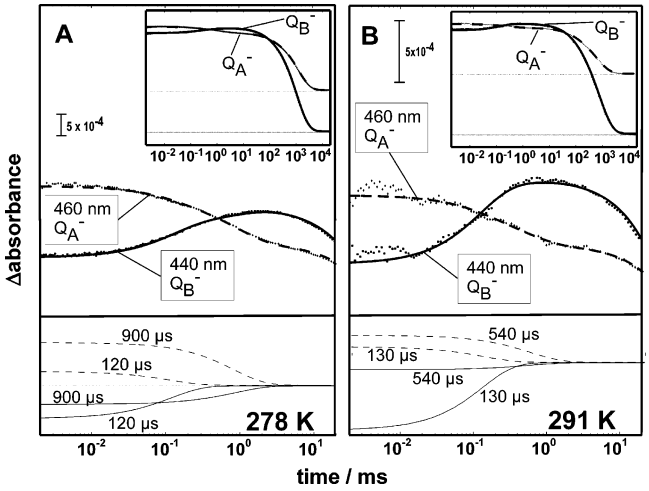

FIGURE 4: Flash-induced absorption transients of RC containing Fe at 440 nm and at 460 nm. Top: Experimental data are shown as dots and fitting curves as lines. Bottom: Respective contributions of the individual exponential phases in the micro- to millisecond time range to the absorbance changes at 440 nm (solid lines) and at 460 nm (dashed lines). (A) Experiment at 278 K; 400 measurements were averaged. Rate constants $\tau_1 = 120$ μs and $\tau_2 = 900$ μs describe the $Q_A^- \rightarrow Q_B$ electron transfer step. (B) Experiment at 291 K; 300 measurements were averaged. The respective rate constants are $\tau_1 = 130$ μs and $\tau_2 = 540$ μs. Inset: Absorbance changes for Q_A^- and Q_B^- marker bands from 2 μs to 20 s. Dotted hairlines indicate absorption zero lines of the individual curves. For the fitting curves shown in the top panels further kinetic components in the hundreds of milliseconds time range were employed to account for the slower decay of the experimental absorption transients due to Q_A^-/P^+ and Q_B^-/P^+ charge recombination. The initial amplitudes of the absorbance changes, at ~5 μs after the laser flash, predominantly reflect P^+ formation superimposed on smaller Q_A^- contributions. The different initial amplitudes at 278 and 291 K result from different BRC protein concentrations in the measurements.

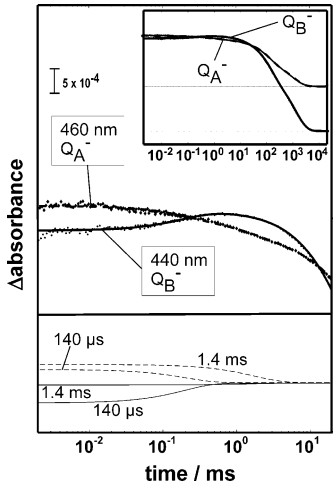

FIGURE 5: Flash-induced absorption transients of Mn-containing RC samples at 440 nm and at 460 nm. Top: Experimental data are shown as dots and fitting curves as lines. Bottom: Respective contributions of the individual exponential phases in the micro- to millisecond time range to the absorbance changes at 440 nm (solid lines) and at 460 nm (dashed lines). Experiment at 278 K; 100 measurements were averaged. Time constants $\tau_1 = 140$ μs and $\tau_2 = 1.4$ ms describe the $Q_A^- \rightarrow Q_B$ electron transfer step. Inset: Absorbance changes for Q_A^- and Q_B^- marker bands from 1 μs to 20 s. The different initial amplitudes with respect to the data in Figure 4 result from different BRC protein concentrations in the measurements.

$Q_A^- \rightarrow Q_B$ transition by VIS absorption spectroscopy. The situation is more difficult in the visible spectral range than in the IR where sharp bands are observed. In the VIS the absorption spectrum of the quinone bound at Q_A overlaps with the one of the quinone bound at Q_B. The electronic absorption difference spectrum $Q_A^-Q_B$ minus $Q_AQ_B^-$ indicates that around 440 nm spectral contributions from Q_B^- are slightly larger than those from Q_A^- whereas at 460 nm the opposite situation is realized (*32*).

Flash-induced absorption transients of wild-type BRC at 278 K, a similar temperature as used in the previous FTIR experiments (*7*), are shown in Figure 4A. Kinetic analyses using a global fit approach (*33*) resolves the different contributions of the kinetic components with apparent time constants as shown in the lower part of Figure 4. It is revealed that the absorbance change at 440 nm attributed to Q_B^- formation is mainly described by a time constant of $\tau_1 = 120$ μs, whereas a decaying component of the 460 nm transient attributed to Q_A^- oxidation is dominated by $\tau_2 = 900$ μs. Because the fit provides apparent time constants and not intrinsic time constants and Q_A^- and Q_B^- absorption bands overlap, both the 120 and the 900 μs components contribute at 440 and 460 nm. However, for a direct transfer from Q_A^- to Q_B the 120 μs component should dominate the Q_A^- disappearance and the Q_B^- appearance, which is obviously not the case. The respective time constants were similar, although slightly smaller than those previously obtained by FTIR (*7*). The temperature of the sample holder as given in the FTIR measurements deviates at the sample on the IR window and is slightly different to the VIS experiments. At the same temperature as used for XAS, namely, 291 K, with liquid BRC solution Q_B^- formation was similarly rapid, occurring with $\tau_1 = 130$ μs. The decay of Q_A^- was still slower than Q_B^- formation and significantly faster than at 278 K, showing a dominant phase with $\tau_2 = 540$ μs (Figure 4B). At room temperature, apparently the two processes are more difficult to separate kinetically than at lower temperature. This may explain why former VIS studies favored the most straightforward interpretation, namely, a direct Q_A^- to Q_B transition. However, our VIS data do not contradict the IR data as argued before but are in reasonable agreement.

In addition to wild-type RC preparations we examined RC samples where the Fe was replaced by manganese. The redox potential of Mn(II) is supposed to be different from that of Fe(II) so that if Fe was involved in the wild type, a different redox behavior may be expected in Mn-containing RC. Figure 5 shows absorption transients at 278 K of Mn-containing RC samples at 440 and 460 nm. We observe the Q_A^- to Q_B transition in the Mn-containing RC at similar kinetics as compared to the RC with Fe. Analysis of the kinetic components at 440 nm shows Q_B^- formation at mainly $\tau_1 = 140$ μs, whereas the decay of the 460 nm transient attributed to Q_A^- oxidation reveals a time constant of $\tau_2 = 1.4$ ms. This result independently supports the conclusion that Fe is not the intermediary electron donor to Q_B and shows even more clearly the kinetic separation of Q_B reduction and the succeeding oxidation of Q_A^-.

DISCUSSION

Recent FTIR experiments have revealed reduction of Q_B within ~150 μs prior to Q_A^- oxidation within about 1 ms (*7*). Therefore, an intermediary redox component must be

involved in the Q_A^- to Q_B transition. It has been suggested, on the basis of the structural arrangement shown in Figure 1, that a possible candidate for such an intermediary electron donor is the non-heme iron. This Fe may transiently undergo an Fe(II) → Fe(III) transition.

In this study, by an Fe-specific time-resolved X-ray absorption experiment we investigated, for the first time directly, whether the Fe(II) becomes transiently oxidized during the $Q_A^- \rightarrow Q_B$ transition. A shift of the Fe K-edge by the expected 2−3 eV to higher energies due to Fe oxidation was not observed. We estimate that at the obtained signal-to-noise ratio of the XAS flash experiments and taking into account the partial occupancy of the Q_B site, we should have been able to monitor upshifts by as low as 0.2 eV (see Supporting Information). Such an upshift would correspond to the oxidation of the Fe in only about 10% of the BRC protein. Even such small upshifts were absent in the experimental data. In conclusion, there is no evidence for oxidation of the Fe upon the first electron transfer from Q_A^- to Q_B.

Surprisingly, the X-ray transients seemed to indicate a transient shift of the Fe K-edge by 0.1−0.2 eV to lower energies. This downshift clearly is too small to be attributable to Fe reduction in a major fraction of the reaction centers. It may be caused by small geometry changes in the Fe coordination environment, e.g., slight lengthening of Fe−ligand bonds (*25*). Such changes may result from protonation events in the vicinity of the Fe as induced by the electrostatic effect of the negative charges on the quinones (*2*, *3*, *39*). The kinetics of the observed X-ray transient could indicate protonation events in the microsecond time range. The IR data show protonation of a not yet identified carboxylic acid within 12 μs (*7*). One conceivable option is the protonation of Glu234 which is an Fe ligand. Presumably this would result in the detachment of the protonated oxygen of its carboxylic group from the Fe. The then expected change from a six-coordinated to a five-coordinated Fe indeed may cause an apparent shift of the Fe K-edge to lower energies (*34*, *35*). A transient monodentate Fe ligation by Glu234 being formed and decaying in the micro- to millisecond time range does not contradict its bidentate ligation observed in the steady-state crystal structures of the Q_AQ_B and $Q_AQ_B^-$ states (*36*) of the *Rb. sphaeroides* RC. Clearly, further experiments are advisable to clarify the origin of the X-ray transients. In any event, also the investigation of a RC variant containing Mn instead of Fe showed an intact electron transfer behavior similar to that of the native protein, which supports the notion that the Fe probably is not transiently oxidized.

In summary, most likely the Fe does not act as an intermediary electron donor to Q_B. However, in this study, the existence of an intermediary electron donor seemingly was corroborated by VIS spectroscopy. In agreement with the previous FTIR findings (*7*) the VIS measurements revealed a major apparent time constant attributable to Q_B^- formation, smaller than the major apparent time constant describing Q_A^- decay. Due to broader spectral bands and their significant overlap in the VIS region (*32*), the kinetic components from the two quinones are not as clearly separated as in FTIR spectroscopy (*7*). On the basis of the VIS data alone, one may not propose an intermediary redox compound, but the VIS data do not exclude such an intermediate in contrast to earlier interpretations. The similarity of the kinetics of the FTIR and VIS transients suggests that they are attributable to the same processes. An explanation for the kinetic mismatch in the VIS and FTIR data is that Q_B^- formation precedes Q_A^- reoxidation, necessitating an intermediary redox compound.

All three techniques, namely, optical absorption, FTIR, and, as for the first time demonstrated in this investigation, also X-ray spectroscopy, are suited to follow the reactions at the BRC acceptor side with high time resolution and point to an intermediate in the Q_A^- to Q_B transition. Its nature remains unclear; the most obvious candidate Fe seems to be excluded. Further experiments are in progress in our laboratories to unravel the events that govern the electron transfer reactions involving the quinones.

ACKNOWLEDGMENT

We thank the staff of ID26 at ESRF and in particular Dr. Pieter Glatzel for excellent support, Gabriele Smuda (University Bochum) for technical assistance, Yulia Sandomirskaja (University Bochum) for preparing Figure 1, Dr. Klaus Irrgang (TU-Berlin) for help in AAS, and Dr. Hagen Stosnach from Röntec (Berlin) and Simone Löscher (FU-Berlin) for performing the TXRF measurements. M.H. thanks Prof. Klaus Möbius (FU-Berlin) for an inspiring discussion and Prof. Holger Dau (FU-Berlin) for generous long-term support.

SUPPORTING INFORMATION AVAILABLE

One figure showing X-ray absorption data at the Mn K-edge of the manganese complex of photosystem II. This material is available free of charge via the Internet at http://pubs.acs.org.

REFERENCES

1. Ermler, U., Michel, H., and Schiffer, M. (1994) Structure and function of the photosynthetic reaction center from *Rhodobacter sphaeroides*, *J. Bioenerg. Biomembr. 26*, 5−15.
2. Wraight, C. A. (2004) Proton and electron transfer in the acceptor quinone complex of photosynthetic reaction centers from *Rhodobacter sphaeroides*, *Front. Biosci. 9*, 309−337.
3. Okamura, M. V., Paddock, M. L., Graige, M. S., and Feher, G. (2000) Proton and electron transfer in bacterial reaction centers, *Biochim. Biophys. Acta 1458*, 148−163.
4. Adelroth, P., and Brezezinski, P. (2004) Surface-mediated proton-transfer reactions in membrane-bound proteins, *Biochim. Biophys. Acta 1655*, 102−115.
5. Stowell, M. H., McPhillips, T. M., Rees, D. C., Soltis, S. M., Abresch, E., and Feher, G. (1997) Light-induced structural changes in photosynthetic reaction center: implications for mechanism of electron−proton transfer, *Science 276*, 812−816.
6. Breton, J., Boullais, C., Mioskowski, C., Sebban, P., Baciou, L., and Nabedryk, E. (2002) Vibrational spectroscopy favors a unique Q_B binding site at the proximal position in wild-type reaction centers and in the Pro-L209→Tyr mutant from *Rhodobacter sphaeroides*, *Biochemistry 41*, 12921−12927.
7. Remy, A., and Gerwert, K. (2003) Coupling of light-induced electron transfer to proton uptake in photosynthesis, *Nat. Struct. Biol. 10*, 637−644.
8. Baxter, R. H. G., Ponomarenk, N., Srajer, V., Pahl, R., Moffat, K., and Norris, J. R. (2004) Time-resolved crystallographic studies of light-induced structural changes in the photosynthetic reaction center, *Proc. Natl. Acad. Sci. U.S.A. 101*, 5982−5987.
9. Breton, J. (2004) Absence of large-scale displacement of quinone Q_B in bacterial photosynthetic reaction centers, *Biochemistry 43*, 3318−3326.
10. Pokkuluri, P. R., Laible, P. D., Crawford, A. E., Mayfield, J. F., Yousef, M. A., Ginell, S. L., Hanson, D. K., and Schiffer, M. (2004) Temperature and cryoprotectant influence secondary

quinone binding position in bacterial reaction centers, *FEBS lett. 570*, 171−174.
11. Brudler, R., de Groot, H. J. M., van Liemt, W. B. S., Steggerda, W. F., Esmijer, R., Gast, P., Hoff, A. J., Lugtenburg, J., and Gerwert, K. (1994) Asymmetric binding of the 1- and 4-C═O groups of Q_A in *Rhodobacter sphaeroides* R26 reaction centres monitored by Fourier transform infra-red spectroscopy using site-specific isotopically labelled ubiquinone-10, *EMBO J. 13*, 5523−5530.
12. Brudler, R., de Groot, H. J. M., van Liemt, W. B. S., Gast, P., Hoff, A. J., Lugtenburg, J., and Gerwert, K. (1995) FTIR spectroscopy shows weak symmetric hydrogen bonding of the QB carbonyl groups in *Rhodobacter sphaeroides* R26 reaction centres, *FEBS Lett. 370*, 88−92.
13. Debus, R., Feher, G., and Okamura, M. Y. (1986) Iron-depleted reaction centers from Rhodopseudomonas sphaeroides R-26.1: characterization and reconstitution with Fe^{2+}, Mn^{2+}, Co^{2+}, Ni^{2+}, Cu^{2+}, and Zn^{2+}, *Biochemistry 25*, 2276−2287.
14. Utschig, L. M., and Thurnauer, M. C. (2004) Metal ion modulated electron transfer in photosynthetic proteins, *Acc. Chem. Res. 37*, 439−447.
15. Feher, G., and Okamura, M. Y. (1999) The primary and secondary acceptors in bacterial photosynthesis. II. The structure of the Fe-Q-complex, *Appl. Magn. Reson. 16*, 63−100.
16. Utschig, L. M., Greenfield, S. R., Tang, J., Laible, P. D., and Thurnauer, M. C. (1997) Influence of iron-removal procedures on sequential electron transfer in photosynthetic bacterial reaction centers studied by transient EPR spectroscopy, *Biochemistry 36*, 8548−8558.
17. Averill, B. A., and Vincent, J. B. (1993) Electronic absorption spectroscopy of nonheme iron proteins, *Methods Enzymol. 226*, 33−51.
18. Krebs, C., Price, J. C., Baldwin, J., Saleh, L., Green, M. T., and Bollinger, J. M., Jr. (2005) Rapid freeze-quench ^{57}Fe Mössbauer spectroscopy: monitoring changes of an iron-containing active site during a biochemical reaction, *Inorg. Chem. 44*, 742−757.
19. Butler, W. F., Calvo, R., Fredkin, D. R., Isaacson, R. A., Okamura, M. Y., and Feher, G. (1984) The electronic structure of Fe^{2+} in reaction centers from *Rhodopseudomonas sphaeroides*. III. EPR measurements of the reduced acceptor quinones, *Biophys. J. 45*, 947−973.
20. Haumann, M., Müller, C., Liebisch, P., Neisius, T., and Dau, H. (2005) A novel BioXAS technique with microsecond time resolution to track oxidation state and structural changes at biological metal centers−S-state transitions of the manganese complex of oxygenic photosynthesis, *J. Synchrotron Radiat. 12*, 35−44.
21. Straley, S. C., Parson, W. W., Mauzerall, D., and Clayton, R. K. (1973) Pigment content and molar extinction coefficients of photochemical reaction centers from *Rhodopseudomonas sphaeroides*, *Biochim. Biophys. Acta 305*, 597−609.
22. Okamura, M. Y., Debus, R. J., Kleinfeld, D., and Feher, G. (1982) in *Function of Quinones in Energy Conserving Systems* (Trumpower, B. L., Ed.) pp 299−317, Academic Press, New York.
23. Sole, V. A., Gauthier, C., Goulon, J., and Natoli, F. (1999) Undulator QEXAFS at the ESRF beamline ID26, *J. Synchrotron Radiat. 6*, 174−175.
24. Dau, H., and Haumann, M. (2003) X-ray absorption spectroscopy to watch catalysis by metalloenzymes−Status and perspectives discussed for the water-splitting manganese complex of photosynthesis, *J. Synchrotron Radiat. 10*, 76−85.
25. Dau, H., Liebisch, P., and Haumann, M. (2003) X-ray absorption spectroscopy to analyze nuclear geometry and electronic structure of biological metal centers−Potential and questions examined with special focus on the tetranuclear manganese complex of oxygenic photosynthesis, *Anal. Bioanal. Chem. 376*, 562−583.
26. Kleinfeld, D., Okamura, M. Y., and Feher, G. (1984) Electron transfer in reaction centers of *Rhodopseudomonas sphaeroides*. I. Determination of the charge recombination pathway of D+QAQ-(−)B and free energy and kinetic relations between Q(−)AQB and QAQ(−)B, *Biochim. Biophys. Acta 766*, 126−140.
27. Francia, F., Palazzo, G., Mallardi, A., Cordone, L., and Venturoli, G. (2003) Residual water modulates Q_A^- to Q_B^- electron transfer in bacterial reaction centers embedded in trehalose amorphous matrices, *Biophys. J. 85*, 2760−2775.
28. Bunker, G., Stern, E. A., Blankenship, R. E., and Parson, W. W. (1982) An X-ray absorption study of the iron site in bacterial photosynthetic reaction centers, *Biophys. J. 37*, 539−551.
29. Eisenberger, P., Okamura, M. Y., and Feher, G. (1982) The electronic structure of the Fe^{2+} in reaction centers from *Rhodopseudomonas sphaeroides*, *Biophys. J. 37*, 523−538.
30. Shearer, J., Scarrow, R. C., and Kovacs, J. A. (2002) Synthetic models for the cysteinate-ligated non-heme iron enzyme superoxide reductase: observation and structural characterization by XAS of an Fe(III)-OOH intermediate, *J. Am. Chem. Soc. 124*, 11709−11717.
31. Haumann, M., Liebisch, P., Müller, C., Barra, M., Grabolle, M., and Dau, H. (2005) Photosynthetic O_2-formation tracked by time-resolved X-ray experiments, *Science 310*, 1019−1021.
32. Li, J., Gilroy, D., Tiede, D. M., and Gunner, M. R. (1998) Kinetic phases in the electron transfer from $P^+Q_A^-Q_B$ to $P^+Q_AQ_B^-$ and the associated processes in *Rhodobacter sphaeroides* R-26 reaction centers, *Biochemistry 37*, 2818−2829.
33. Hessling, B., Souvignier, G., and Gerwert, K. (1993) A model-independent approach to assigning bacteriorhodopsin's intramolecular reactions to photocycle intermediates, *Biophys. J. 65*, 1929−1941.
34. Dau, H., Liebisch, P., and Haumann, M. (2005) The manganese complex of oxygenic photosynthesis: Conversion of five-coordinated Mn(III) to six-coordinated Mn(IV) in the S_2-S_3 transition is implied by XANES simulations, *Phys. Scripta T115*, 844−846.
35. Burgdorf, T., Löscher, S., Liebisch, P., van der Linden, E., Galander, M., Lendzian, F., Albracht, S. P., Meyer-Klaucke, W., Friedrich, B., Dau, H., and Haumann, M. (2005) Structural and oxidation state changes at its non-standard Ni−Fe site during activation of the NAD-reducing hydrogenase from *Ralstonia eutropha* detected by X-ray absorption, EPR, and FTIR spectroscopy, *J. Am. Chem. Soc. 127*, 576−592.
36. Stowell, M. H., McPhillips, T. M., Rees, D. C., Soltis, S. M., Abresch, E., and Feher, G. (1997) Light-induced structural changes in photosynthetic reaction center: implications for mechanism of electron−proton transfer, *Science 276*, 812−806.
37. Gerencser, L., Taly, A., Baciou, L., Maroti, P., and Sebban, P. (2002) Effect of binding of Cd^{2+} on bacterial reaction center mutants: Proton transfer uses interdependent pathways, *Biochemistry 41*, 9132−9138.
38. Klockenkämper, R. (1996) *Total Reflection X-ray Fluorescence Analysis*, Wiley, London, U.K.
39. Ishikita, H., and Knapp, E. W. (2005) Oxidation of the non-heme iron complex in photosystem II, *Biochemistry 44*, 14772−14783.

BI0515725